

Can experimentally-accessible measures of entanglement distinguish quantum spin liquids from disorder-driven “random singlet” phases ?

Tokuro Shimokawa,^{1,*} Snigdha Sabharwal,¹ and Nic Shannon¹

¹Theory of Quantum Matter Unit, Okinawa Institute of Science and Technology Graduate University, Onna-son, Okinawa 904-0412, Japan
(Dated: June 12, 2025)

At the theoretical level, quantum spin liquids are distinguished from other phases of matter by their entanglement properties. However, since the usual measure of entanglement, entanglement entropy, cannot be accessed in experiment, identifying quantum spin liquids in candidate materials remains an acute problem. Here we show other, experimentally-accessible, measures of entanglement can be used to distinguish a quantum spin liquid from a competing disorder-driven “random singlet” phase, in a model of a disordered antiferromagnet on a triangular lattice. The application of these results to the triangular-lattice systems YbZnGaO₄, YbZn₂GaO₅ and KYbSe₂ is discussed.

Half a century has passed since Anderson pioneered resonating valence bonds (RVB) as an alternative to low-temperature magnetic order [1], paving the way for the modern concept of a quantum spin liquid (QSL) [2]. In that time, the study of QSL has become a central topic in condensed matter physics [3–6], with important connections to both quantum computing [7], and high-energy physics [8]. None the less, the identification of QSL in experiment remains a challenge, particularly in materials with chemical or structural disorder, where there can be many different routes to a spin-disordered ground state [9–24].

In many cases, the sharpest distinction between conventional and unconventional phases of matter such as QSL lies in their entanglement properties [4, 25–27]. This fact has been put to good use in simulation [20, 28], but when it comes to candidate materials, this approach is more challenging, since the entanglement entropy and entanglement spectra studied in simulation are not, in general, accessible to experiment [29]. None the less, there are alternative measures or “witnesses” of entanglement which can be measured [30]. Recent experiments have demonstrated the potential of this approach in context of molecular qubits [31], quasi-one dimensional spin chains [32–34], and triangular-lattice antiferromagnets [35–37]. However the signal properties of entanglement witnesses in spin models remain relatively unexplored, particularly when it comes to systems with disorder [38]. And an important question, in this context, is how we could experimentally distinguish a QSL from the disorder-driven phases found in systems with strongly disordered interactions [9, 12, 16, 17, 19, 21, 38–53].

In this Letter, we show that experimentally-accessible measures of entanglement can distinguish a quantum spin liquid from the disorder-driven “random singlet” phase in a representative model of a triangular lattice antiferromagnet. The measures we consider are concurrence, and the closely related two-tangle [54–56], and quantum Fisher information [57–59], both of which have previously been discussed in the context of inelastic neutron scattering or muon spin relaxation experiments [30–33, 35–37, 60, 61]. These are calculated at finite temperature, within a quantum typicality approach derived

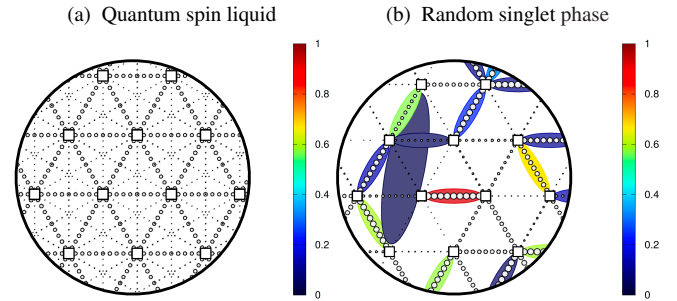


Figure 1. Singular difference in pairwise entanglement found in quantum spin liquid (QSL) and disorder-driven “random singlet” (RS) phases on a triangular lattice. (a) Concurrence C_{ij} within QSL phase, showing that the entanglement between any pair of spins is identically zero. (b) Equivalent results within RS phase, showing irregular pattern of entanglement between pairs of spins on different lengthscales. Results are taken from zero-temperature exact diagonalization (ED) calculations for a cluster of 30 spins, for the disordered triangular-lattice antiferromagnet [Eq. (1)], with parameters [Eq. (3)], as described in the text. The relative strength of interactions on different bonds is shown through thickness of dashed lines.

from exact diagonalization [62–64]. We find that both RS and QSL phases exhibit multipartite entanglement, but show very different characteristics in pairwise entanglement, as measured through concurrence [Fig. 1]. While the temperature-dependence of the two-tangle (or concurrence) clearly distinguishes RS from QSL phases in simulation, we conclude that these measures of entanglement cannot be safely inferred from experiments on disordered systems [Fig. 3]. In contrast, we find that the temperature-dependence of quantum Fisher information (QFI) provides a robust tool for distinguishing RS from QSL states in triangular-lattice antiferromagnets [Fig. 4]. We discuss the implication of these results for experiment, finding evidence in support of spin liquid scenario for YbZnGaO₄ [35] and YbZn₂GaO₅ [37], and showing that the properties of KYbSe₂ [36] are consistent with proximity to a quantum critical point [Fig. 5].

Model and materials. The competition between Néel, QSL and disorder-driven “random singlet” phases has been widely discussed in the context of triangular-lattice antiferromagnets (AF) based on (pseudo)spin-1/2 Yb³⁺ ions [65, 66], includ-

* tokuro.shimokawa@oist.jp

ing NaYbS₂ [67, 68], NaYbO₂ [69, 70], NaYbSe₂ [71, 72], RbYbSe₂ [73], CsYbSe₂ [74] and YbZn₂GaO₅ [37]. A prototypical example is YbMgGaO₄, originally proposed as a QSL [75–83], which has since been argued to exhibit a disorder-driven state mimicking the correlations of a QSL [14, 16, 84].

Isostructural YbZnGaO₄ has been discussed as both a QSL [35, 37] and a spin glass [85]. Meanwhile KYbSe₂ exhibits Néel order, but has been argued to lie close to a quantum critical point (QCP) separating this from a QSL [33].

With these results in mind, we consider the model most commonly used to interpret experiments on these materials,

$$\mathcal{H} = J_1 \sum_{\langle ij \rangle_1} (1 + \Delta \alpha_{ij}) \mathbf{S}_i \cdot \mathbf{S}_j + J_2 \sum_{\langle ij \rangle_2} (1 + \Delta \beta_{ij}) \mathbf{S}_i \cdot \mathbf{S}_j, \quad (1)$$

where interactions on 1st- and 2nd-neighbour bonds of a triangular lattice are subject to quenched random disorder of strength Δ , drawn from a uniform distribution

$$\alpha_{ij}, \beta_{ij} \in [-1, 1]. \quad (2)$$

In Fig. 2 we show a schematic phase diagram of the model Eq. (1), based on previous studies with [9, 11, 20], and without [76, 86–93], disorder. Interactions are shown schematically in an inset. In the absence of disorder ($\Delta = 0$), the model supports 3-sublattice coplanar Néel order for small J_2/J_1 [94], and 2-sublattice collinear “stripe” order for large J_2/J_1 [95, 96]. A quantum spin liquid (QSL), which may be gapless [86, 91, 92, 97], or possess a small gap [87, 88, 90, 93], has been identified at intermediate parameters [98]. In the presence of disorder $\Delta > 0$, both QSL and ordered phases give way to a disorder-driven state which can mimic many of the properties of the QSL [9, 20], here labelled “RS”.

In one dimension (1D), bond-disorder of the type found in Eq. (1) gives rise to a “random-singlet” (RS) phase whose long-distance properties are controlled by singlets formed at exponentially-long length scales [39, 40]. The RS phase mimics a number of the properties of the critical Luttinger liquid (1D QSL) found in spin chains without disorder, including an algebraic $1/r^2$ decay of correlations, and logarithmic growth of entanglement entropy $S_E \sim \log L$ [28, 38, 99]. None the less it represents an entirely distinct phase of matter, lacking the conformal invariance and coherent fractionalized excitations (spinons) of the Luttinger liquid, and instead having properties controlled by the fixed point of a strong-disorder renormalization group (SDRG) [40].

The situation for disordered magnets in two dimensions (2D) is much less clear. Early arguments of Imry and Ma suggest that disorder can have singular effect on gapless ordered states in 2D [100], while SDRG calculations identify a potential fixed point with spin glass character [44, 45, 53], and a number of other scenarios have also been discussed [16, 41–44, 46–52]. Meanwhile numerical calculations for frustrated magnets with bond disorder [9–12, 14, 15, 17–21, 23] find disorder-driven states which can mimic both the thermodynamic properties of gapless QSL, $C(T \rightarrow 0) \propto T^\alpha$ [10], and the diffuse structures found in the correlations $S(\mathbf{q})$ [10, 14, 16]. Results for different models display a number of

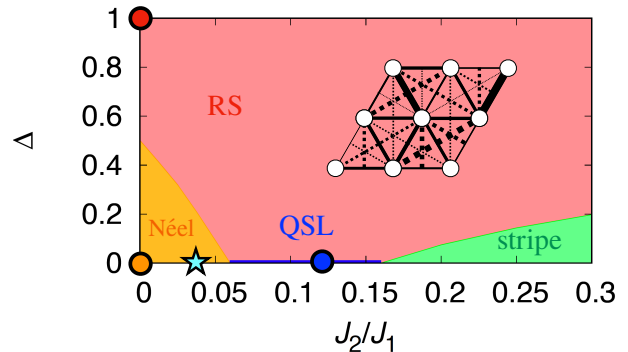


Figure 2. Schematic ground state phase diagram for the spin-1/2 J_1 - J_2 antiferromagnet on a triangular lattice, as a function of bond-disorder. In the absence of disorder ($\Delta = 0$), ordered antiferromagnetic “Néel” and “stripe” phases are separated by a region where the ground state is identified as a quantum spin liquid (QSL). In the presence of disorder ($\Delta > 0$), these phases give way to a disorder-driven state which can mimic many of the properties of the QSL, denoted here as “random singlet” (RS) phase. Phase boundaries reflect the general trends in published results for the model [Eq. (1)], in the presence [9, 20] and absence [76, 86–88] of disorder. The inset illustrates interactions J_1 (solid lines) and J_2 (dashed lines) at finite Δ , with the thickness of the line reflecting the strength of the interaction. Parameter sets considered in this paper [Eq. (3)] are shown with circles. A star denotes parameters proposed for KYbSe₂ [36].

common features, including the presence of “random” (static) singlet bonds over multiple length scales and the existence of orphaned spins [10, 16]. None the less, the general classification of numerical results in terms of RG fixed points remains an open problem. Here, we follow [9–11, 17, 21] in using the term “random singlet” (RS) phase to describe the disorder-driven phase we study, without seeking to identify this with any particular fixed point.

For purposes of numerical study, we select parameters characteristic of the Néel, QSL and RS phases

$$\bullet \quad (J_1, J_2, \Delta) = (1, 0, 0) \quad [\text{Néel}] \quad (3a)$$

$$\bullet \quad (J_1, J_2, \Delta) = (1, 0.12, 0) \quad [\text{QSL}] \quad (3b)$$

$$\bullet \quad (J_1, J_2, \Delta) = (1, 0, 1) \quad [\text{RS}] \quad (3c)$$

as shown in Fig. 2. We also consider one parameter set taken from experiments on KYbSe₂ [36, 101]

$$\star \quad (J_1, J_2, \Delta) = (1, 0.047, 0) \quad [\text{KYbSe}_2] \quad (4)$$

Numerical simulations of Eq. (1) were carried out for clusters of $N = 18, 24, 30$ spins, using exact diagonalization (ED) at $T = 0$ and thermal pure quantum state (TPQ) methods at finite T , as described in the Supplemental Material [102].

Entanglement measures. We consider three different measures of entanglement concurrence, two-tangle, and quantum Fisher information. Since these measures apply to mixed states, and can be expressed in terms of two-point spin correlation functions, they are, *a priori*, directly applicable to experiment [30–32, 35, 36]. The definitions given below apply to systems model with (at least) $U(1)$ spin-rotation symmetry; further details can be found in two recent reviews [60, 61].

Concurrence:

$$C_{ij} = 2 \max\left\{0, \sqrt{(\langle S_i^x S_j^x \rangle + \langle S_i^y S_j^y \rangle)^2} - \sqrt{\left(\frac{1}{4} + \langle S_i^z S_j^z \rangle\right)^2 - \left(\frac{\langle S_i^z \rangle + \langle S_j^z \rangle}{2}\right)^2}\right\}, \quad (5)$$

provides a quantitative measure of the entanglement between a given pair of spins, with $C_{ij} \in [0, 1]$ where 0 signals a separable state, and 1 maximal entanglement [54–56].

Two-tangle:

$$\tau_j^{(2)} = \sum_{i \neq j} C_{ij}^2, \quad (6)$$

is derived from concurrence, and quantifies the total two–spin entanglement associated with a spin on site j [54–56].

Quantum Fisher information density ($nQFI$):

$$f_{\mathcal{Q}}[\mathbf{q}, T] = 4 \int_0^\infty d\omega \tanh\left(\frac{\omega}{2T}\right) (1 - e^{-\beta\omega}) S^{zz}(\mathbf{q}, \omega, T), \quad (7)$$

is defined in terms of a dynamical structure factor (here, $S^{zz}(\mathbf{q}, \omega, T)$), and provides a lower bound on the depth of entanglement associated with fluctuations at a given wavevector \mathbf{q} . More concretely, when $f[\mathbf{q}, T] > m$ (where m is a positive integer and a divisor of N), the quantum state in question is at least $m + 1$ multipartite entangled [57–59, 103, 104].

Concurrence as measured by experiment:

$$\tilde{C}_{ij} = 2 \max\left\{0, \sqrt{(\overline{\langle S_i^x S_j^x \rangle} + \overline{\langle S_i^y S_j^y \rangle})^2} - \sqrt{\left(\frac{1}{4} + \overline{\langle S_i^z S_j^z \rangle}\right)^2 - \left(\frac{\overline{\langle S_i^z \rangle} + \overline{\langle S_j^z \rangle}}{2}\right)^2}\right\}. \quad (8)$$

In theoretical calculations, these measures of entanglement can straightforwardly be generalized to systems with disorder by taking averages of Eq. (5), Eq. (6) and Eq. (7) within an ensemble of disordered states. We denote these as quantities as \overline{C}_{ij} , $\overline{\tau}^{(2)}$ and $\overline{f_{\mathcal{Q}}}$, respectively. However when evaluating entanglement measures from experiment, it is instead the disorder-averaged correlation of spins $\overline{\langle S_i^\alpha S_j^\alpha \rangle}$ which enters calculations, leading to Eq. (8). This difference in the order of averages has profound implications for the values of concurrence in the presence of disorder, a point discussed at length in [38].

Results for concurrence. The singular difference between the entanglement structure of the QSL and RS phases is evident at the level of the two–spin entanglement probed by concurrence. In Fig. 1 we show results for C_{ij} [Eq. (5)] in QSL and RS ground states, where results for the RS are shown for a single realization of disorder. Concurrence within the QSL vanishes identically, reflecting the fact that its entanglement is of a profoundly multipartite nature. The RS phase also possess multipartite entanglement, as evidenced by the residual tangle, discussed in [102], and the QFI, discussed below.

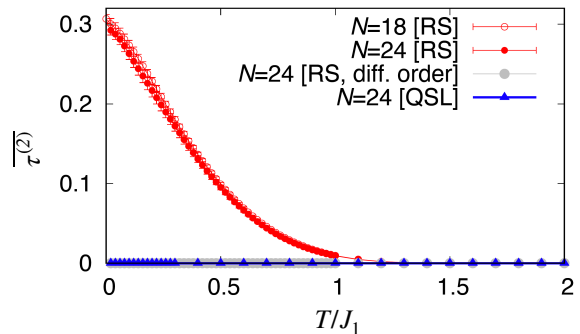


Figure 3. Temperature dependence of the two–tangle in the quantum spin liquid (QSL) and disorder–driven random singlet (RS) phases. The two–tangle [Eq. (9)], averaged over different disorder realizations, takes on a finite value $\overline{\tau}^{(2)} > 0$ in the RS phase (red symbols), but vanishes exactly in the QSL (blue symbols), consistent with results for concurrence at $T = 0$, shown in Fig. 1. However if concurrence \tilde{C}_{ij} is calculated using the disorder-averaged spin configurations measured in experiment [Eq. (8)], the resulting estimate of two–tangle also vanishes in the RS phase (grey symbols). Results are taken from quantum typicality (TPQ) calculations for [Eq. (1)], with parameters [Eq. (3)], as described in the text.

None the less, individual spins retain the freedom to form singlets with other spins. These singlets occur at different length scales, with singlets on 1^{st} –neighbour bonds only weakly correlated with the strength of interactions on that bond.

Results for two tangle. At high temperatures, the (deeply) entangled QSL and RS ground states must ultimately give way to a trivial paramagnetic phase, without entanglement. In Fig. 3, we compare results for the temperature dependence of the two–tangle

$$\tau^{(2)} = \frac{1}{N} \sum_i \tau_i^{(2)} \quad (9)$$

in the QSL and RS phases, where results for the RS have been averaged over multiple realizations of disorder. For this order of averages, we recover the behavior expected from ground state correlations, with results for the QSL vanishing identically, and the two–spin entanglement of RS saturating at a finite value for $T \rightarrow 0$. However, if the order of averages is reversed, to reflect the correlations measured in experiment [Eq. (8)], results for the two–tangle also vanish in the RS phase.

The quenching of the two–tangle by disorder is a direct consequence of the convex roof function used in the definition of concurrence [38]. It follows that experimental measurements systematically underestimate the value of concurrence, relative to the Eq. (5), and must be approached with extreme caution. For this reason, in what follows below, we pursue other measures which are reliably accessible in experiment. None the less, concurrence, two tangle and the closely related one–tangle [54–56], remain useful tools for interpreting simulations results. As a practical example, in [102], we show how these measures can be used to determine the phase boundary between Néel and RS phases found in diagonalization calculations for Eq. (1) [cf. Fig. 2].

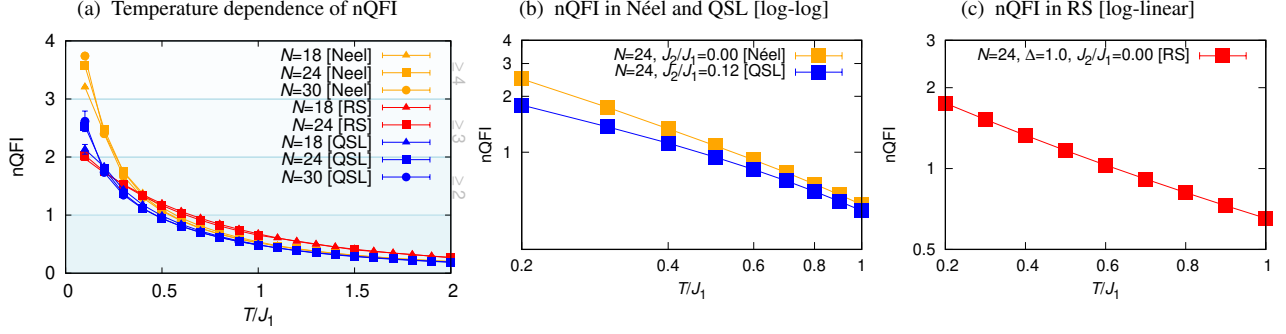


Figure 4. Evolution of multipartite entanglement in Néel, QSL and RS phases as a function of temperature, as witnessed by the quantum Fisher information density (nQFI). (a) Comparison of the temperature–dependence of nQFI [Eq. (7)] for the three different phases. In all cases, multipartite entanglement $m \geq 2$ is present at low temperature. However results for the RS follow a different trajectory from those of the Néel and QSL phases. (b) Results for the Néel and QSL phases replotted on a log–log scale, showing the power–law growth of the depth of entanglement as $T \rightarrow 0$ [Eq. (11)]. (c) Results for the RS phase replotted on a semi–log scale, showing exponential suppression of the depth of entanglement with increasing temperature [Eq. (12)]. Results are taken from quantum typicality (TPQ) calculations for [Eq. (1)], with parameters [Eq. (3)], as described in the text. In all cases, results for nQFI were evaluated at the Néel ordering vector \mathbf{q}_K [Eq. (10)].

Results for quantum Fisher information. While concurrence may prove an unreliable witness in disordered materials, no such problems arise in evaluating quantum Fisher information. In Fig. 4 we present results for the quantum Fisher information density, $f_Q[\mathbf{q}, T]$ [Eq. (7)], for parameters representative of Néel, QSL and RS phases [Eq. (3)]. In all three phases, the dominant two–spin correlations are found at

$$\mathbf{q}_K = \left(\frac{4\pi}{3}, 0 \right) \quad (10)$$

[102], and we therefore use this wavevector in calculating quantum Fisher information. In all cases, the depth of entanglement grows at low temperatures, with all three phases showing (at least) 3–partite entanglement at the lowest temperatures considered [Fig. 4a]. However, while results suggest that the depth of entanglement in both the Néel and QSL phases diverges as $T \rightarrow 0$, the temperature dependence in RS is qualitatively different, and consistent with saturation to a finite value for $T \rightarrow 0$.

We find that data for Néel and QSL are consistent with a power law divergence at low temperatures [Fig. 4b],

$$f_Q[\mathbf{q}_K, T/J_1] \propto b(T/J_1)^{-c} \text{ [Néel, QSL] }, \quad (11)$$

while data for the RS exhibit exponential decay with increasing temperature [Fig. 4c],

$$f_Q[\mathbf{q}_K, T/J_1] \propto b'e^{-c'(T/J_1)} \text{ [RS] }. \quad (12)$$

The distinction between power law and exponential decay of QFI as function of temperature marks a sharp, qualitative, difference QSL and RS which could be used to distinguish them in experiment.

Comparison with experiment. QFI has been measured in three different triangular–lattice AF’s: YbZnGaO₄ [35] and YbZn₂GaO₅ [37], through muon spin rotation (μ SR); and KYbSe₂, through inelastic neutron scattering (INS) [33]. In Fig. 5a we show results for the scaling of the QFI density

found in these experiments, and in simulations for the parameter set proposed for KYbSe₂ [Eq. (4)]. In all three cases we find evidence for a power–law divergence in nQFI at low temperature [Eq. (11)], consistent with simulation results for Néel and QSL phases [Fig. 4b]. We draw two conclusions from these results:

1. The temperature–dependence of nQFI measured in KYbSe₂ is consistent with the observed Néel order.
2. The temperature–dependence of nQFI measured in YbZnGaO₄ and YbZn₂GaO₅ distinguishes in favour of a QSL scenario, and against a RS scenario for these materials.

Connections with quantum criticality. The power–law scaling seen in nQFI [Eq. (11)], is reminiscent of critical phenomena in the limit where $T_c \rightarrow 0$, i.e. approaching a quantum critical point (QCP) [105–107]. In [36], it was found that the dynamical structure factor measured in KYbSe₂ [Fig. 5b] collapses onto a single function

$$T^\alpha S(\mathbf{q}_K, \omega, T) = \Phi \left(\frac{\hbar\omega}{k_B T} \right), \quad (13)$$

[Fig. 5c], a result which was interpreted in terms of proximity to a QCP. In Fig. 5d we show simulation results for $S(\mathbf{q}_K, \omega, T)$, for a cluster of $N = 30$ spins with parameters taken from experiments on KYbSe₂ [Eq (4)]. Simulation results also exhibit a scaling collapse of the form Eq. (13), over a range of ω/T determined by the size of cluster (scatter of points at small ω/T), and the timestep used in simulations, (suppression of response at large ω/T) [Fig. 5e]. A good collapse can be obtained using the exponent reported from experiment $\alpha = 1.73$ [36]. These results lends support to the scenario that the properties of KYbSe₂ are influenced by a nearby QCP [108].

Conclusions. In this Letter we have addressed the question of whether experimentally–accessible measures of entanglement can distinguish quantum spin liquids (QSL) from

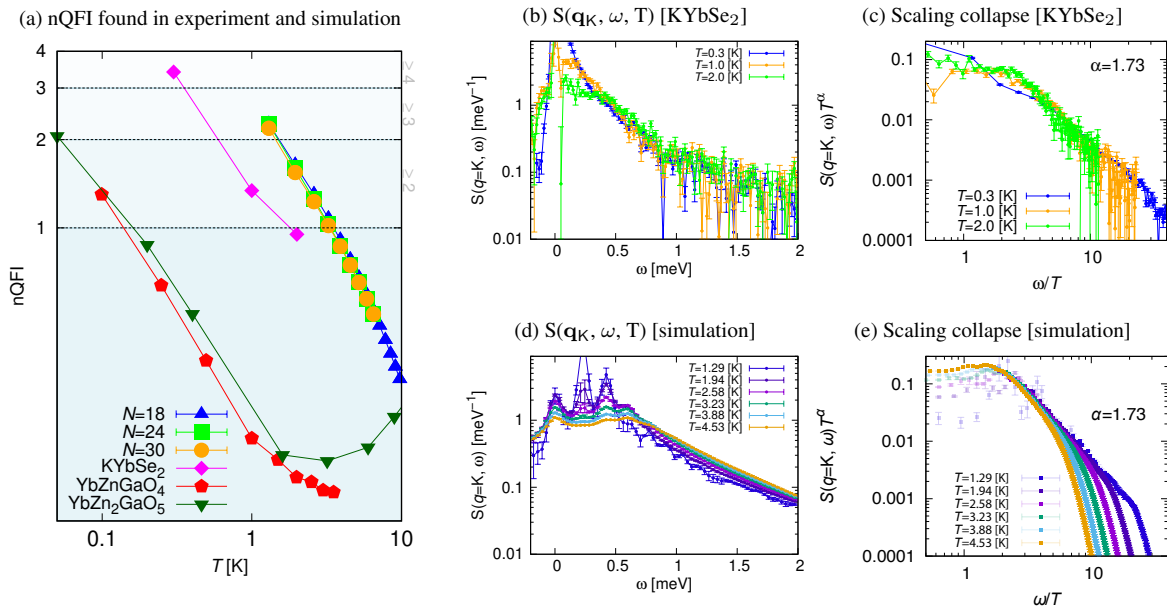


Figure 5. Comparison of results for quantum Fisher information density, and scaling collapse of dynamical susceptibility, as found in simulation and experiment. (a) Quantum Fisher information density (nQFI) as found in simulation, and experiments on KYbSe₂ [36], YbZnGaO₄ [35] and YbZn₂GaO₅ [37]. Both theory and experiment are consistent with a depth of entanglement which diverges as a power law for $T \rightarrow 0$, characteristic of quantum spin liquid (QSL) and Néel phases. (b) Evolution of dynamical structure factor of KYbSe₂ as function of temperature [36]. (c) Scaling collapse of experimental data as a function of ω/T , consistent with the form expected near a quantum critical point (QCP). (d) Evolution of dynamical structure factor found in simulation as function of temperature. (e) Scaling collapse of simulation data. Simulation results are taken from quantum typicality (TPQ) calculations for [Eq. (1)], with parameters [Eq. (4)], as described in the text. In all cases, fluctuations were evaluated at the Néel ordering vector \mathbf{q}_K [Eq. (10)].

disorder-driven “random singlet” (RS) phases. We have addressed this question in the context of model motivated by Yb-based triangular lattice antiferromagnets, which have been proposed as QSL candidates, and where the effects of disorder have also been called into question. And in this context, we find that the answer is “yes”: the way in which the depth of entanglement grows as temperature is reduced, witnessed by the quantum Fisher information (QFI), sharply distinguishes QSL [Fig. 4b] from RS [Fig. 4c] phases.

These results can be compared directly with measurements of QFI in triangular lattice antiferromagnets YbZnGaO₄ [35] and YbZn₂GaO₅ [37], where they provide evidence in support of a QSL [Fig. 5a]. We also revisit experiments on KYbSe₂ [36], finding results consistent with Néel order, proximate to a quantum critical point [Fig. 5]. These findings confirm the utility of measures of entanglement as a practical tool for distinguishing QSL phases in experiment.

Acknowledgments.— This work was supported by the

Theory of Quantum Matter Unit of the Okinawa Institute of Science and Technology Graduate University (OIST), and is also supported by JSPS Grant-in-Aid for Scientific Research (C) Grants No. 21K03477, 25K07213 and MEXT Grant-in-Aid for Transformative Research Areas A “Extreme Universe” Grant No. 22H05266 and 24H00974. The authors are pleased to acknowledge helpful conversations with Matthias Gohlke, Hikaru Kawamura, Hitoshi Ohta, Pranay Patil, Geet Rakala, and Anders Sandvik, and are grateful to Allen Scheie, Alan Tennant and Francis Pratt for providing the initial inspiration for this research. Numerical calculations were carried out using HPC facilities provided by the Supercomputing Center, ISSP, the University of Tokyo; OIST; and the supercomputer Fugaku, provided by RIKEN through the HPCI System Research project (Project IDs:hp230114, hp240014 and hp250047). T. S. thanks Hiroki Nakano for assistance in using Fugaku.

- [1] P. Anderson, *Materials Research Bulletin* **8**, 153 (1973).
 [2] L. Balents, *Nature* **464**, 199 (2010).
 [3] P. A. Lee, *Science* **321**, 1306 (2008).
 [4] L. Savary and L. Balents, *Reports on Progress in Physics* **80**, 016502 (2016).
 [5] Y. Zhou, K. Kanoda, and T.-K. Ng, *Rev. Mod. Phys.* **89**,

- 025003 (2017).
 [6] J. Knolle and R. Moessner, *Annual Review of Condensed Matter Physics* **10**, 451 (2019), <https://doi.org/10.1146/annurev-conmatphys-031218-013401>.
 [7] A. Kitaev, *Annals of Physics* **321**, 2 (2006), January Special Issue.

- [8] H. Yan, *Phys. Rev. B* **102**, 161119 (2020).
- [9] K. Watanabe, H. Kawamura, H. Nakano, and T. Sakai, *Journal of the Physical Society of Japan* **83**, 034714 (2014), <https://doi.org/10.7566/JPSJ.83.034714>.
- [10] H. Kawamura, K. Watanabe, and T. Shimokawa, *Journal of the Physical Society of Japan* **83**, 103704 (2014), <https://doi.org/10.7566/JPSJ.83.103704>.
- [11] T. Shimokawa, K. Watanabe, and H. Kawamura, *Phys. Rev. B* **92**, 134407 (2015).
- [12] K. Uematsu and H. Kawamura, *Journal of the Physical Society of Japan* **86**, 044704 (2017), <https://doi.org/10.7566/JPSJ.86.044704>.
- [13] J.-J. Wen, S. M. Koohpayeh, K. A. Ross, B. A. Trump, T. M. McQueen, K. Kimura, S. Nakatsuji, Y. Qiu, D. M. Pajerowski, J. R. D. Copley, and C. L. Broholm, *Phys. Rev. Lett.* **118**, 107206 (2017).
- [14] Z. Zhu, P. A. Maksimov, S. R. White, and A. L. Chernyshev, *Phys. Rev. Lett.* **119**, 157201 (2017).
- [15] K. Uematsu and H. Kawamura, *Phys. Rev. B* **98**, 134427 (2018).
- [16] I. Kimchi, A. Nahum, and T. Senthil, *Phys. Rev. X* **8**, 031028 (2018).
- [17] L. Liu, H. Shao, Y.-C. Lin, W. Guo, and A. W. Sandvik, *Phys. Rev. X* **8**, 041040 (2018).
- [18] K. Uematsu and H. Kawamura, *Phys. Rev. Lett.* **123**, 087201 (2019).
- [19] H. Kawamura and K. Uematsu, *Journal of Physics: Condensed Matter* **31**, 504003 (2019).
- [20] H.-Q. Wu, S.-S. Gong, and D. N. Sheng, *Phys. Rev. B* **99**, 085141 (2019).
- [21] L. Liu, W. Guo, and A. W. Sandvik, *Phys. Rev. B* **102**, 054443 (2020).
- [22] K. Seki, T. Hikihara, and K. Okunishi, *Phys. Rev. B* **104**, 134405 (2021).
- [23] K. Uematsu, T. Hikihara, and H. Kawamura, *Journal of the Physical Society of Japan* **90**, 124703 (2021), <https://doi.org/10.7566/JPSJ.90.124703>.
- [24] H.-D. Ren, T.-Y. Xiong, H.-Q. Wu, D. N. Sheng, and S.-S. Gong, *Phys. Rev. B* **107**, L020407 (2023).
- [25] A. Kitaev and J. Preskill, *Phys. Rev. Lett.* **96**, 110404 (2006).
- [26] M. Levin and X.-G. Wen, *Phys. Rev. Lett.* **96**, 110405 (2006).
- [27] N. Laflorencie, *Physics Reports* **646**, 1 (2016), quantum entanglement in condensed matter systems.
- [28] N. Laflorencie, *Phys. Rev. B* **72**, 140408 (2005).
- [29] R. Islam, R. Ma, P. M. Preiss, M. Eric Tai, A. Lukin, M. Rispoli, and M. Greiner, *Nature* **528**, 77 (2015).
- [30] C. Brukner, V. Vedral, and A. Zeilinger, *Phys. Rev. A* **73**, 012110 (2006).
- [31] E. Garlatti, T. Guidi, S. Ansbro, P. Santini, G. Amoretti, J. Olivier, H. Mutka, G. Timco, I. J. Vitorica-Yrezabal, G. F. S. Whitehead, R. E. P. Winpenny, and S. Carretta, *Nature Communications* **8**, 14543 (2017).
- [32] P. Laurell, A. Scheie, C. J. Mukherjee, M. M. Koza, M. Enderle, Z. Tylczynski, S. Okamoto, R. Coldea, D. A. Tennant, and G. Alvarez, *Phys. Rev. Lett.* **127**, 037201 (2021).
- [33] A. Scheie, P. Laurell, A. M. Samarakoon, B. Lake, S. E. Nagler, G. E. Granroth, S. Okamoto, G. Alvarez, and D. A. Tennant, *Phys. Rev. B* **103**, 224434 (2021).
- [34] V. Menon, N. E. Sherman, M. Dupont, A. O. Scheie, D. A. Tennant, and J. E. Moore, *Phys. Rev. B* **107**, 054422 (2023).
- [35] F. L. Pratt, F. Lang, W. Steinhardt, S. Haravifard, and S. J. Blundell, *Phys. Rev. B* **106**, L060401 (2022).
- [36] A. O. Scheie, E. A. Ghioldi, J. Xing, J. A. M. Paddison, N. E. Sherman, M. Dupont, L. D. Sanjeewa, S. Lee, A. J. Woods, D. Abernathy, D. M. Pajerowski, T. J. Williams, S.-S. Zhang, L. O. Manuel, A. E. Trumper, C. D. Pemmaraju, A. S. Sefat, D. S. Parker, T. P. Devereaux, R. Movshovich, J. E. Moore, C. D. Batista, and D. A. Tennant, *Nature Physics* **20**, 74 (2024).
- [37] H. C. H. Wu, F. L. Pratt, B. M. Huddart, D. Chatterjee, P. A. Goddard, J. Singleton, D. Prabhakaran, and S. J. Blundell, “Spin dynamics in the dirac $u(1)$ spin liquid $\text{ybzn}_2\text{ga}_5\text{o}_5$,” (2025), [arXiv:2502.00130 \[cond-mat.str-el\]](https://arxiv.org/abs/2502.00130).
- [38] S. Sabharwal, T. Shimokawa, and N. Shannon, “Witnessing disorder in quantum magnets,” Accepted for publication in *PRResearch* (2024), [arXiv:2407.20797 \[cond-mat.str-el\]](https://arxiv.org/abs/2407.20797).
- [39] C. Dasgupta and S.-k. Ma, *Phys. Rev. B* **22**, 1305 (1980).
- [40] D. S. Fisher, *Phys. Rev. B* **50**, 3799 (1994).
- [41] Y. Nonomura and Y. Ozeki, *Journal of the Physical Society of Japan* **64**, 2710 (1995), <https://doi.org/10.1143/JPSJ.64.2710>.
- [42] J. Oitmaa and O. P. Sushkov, *Phys. Rev. Lett.* **87**, 167206 (2001).
- [43] O. Motrunich, S.-C. Mau, D. A. Huse, and D. S. Fisher, *Phys. Rev. B* **61**, 1160 (2000).
- [44] Y.-C. Lin, R. Mélin, H. Rieger, and F. Iglói, *Phys. Rev. B* **68**, 024424 (2003).
- [45] F. Iglói and C. Monthus, *Physics Reports* **412**, 277 (2005).
- [46] R. Yu, T. Roscilde, and S. Haas, *Phys. Rev. B* **73**, 064406 (2006).
- [47] N. Laflorencie, S. Wessel, A. Läuchli, and H. Rieger, *Phys. Rev. B* **73**, 060403 (2006).
- [48] M. Tarzia and G. Biroli, *Europhysics Letters* **82**, 67008 (2008).
- [49] T. Vojta, A. Farquhar, and J. Mast, *Phys. Rev. E* **79**, 011111 (2009).
- [50] T. Vojta, C. Kotabage, and J. A. Hoyos, *Phys. Rev. B* **79**, 024401 (2009).
- [51] R. R. P. Singh, *Phys. Rev. Lett.* **104**, 177203 (2010).
- [52] C. K. Thomas, D. A. Huse, and A. A. Middleton, *Phys. Rev. Lett.* **107**, 047203 (2011).
- [53] F. Iglói and C. Monthus, *The European Physical Journal B* **91**, 290 (2018).
- [54] V. Coffman, J. Kundu, and W. K. Wootters, *Phys. Rev. A* **61**, 052306 (2000).
- [55] L. Amico, A. Osterloh, F. Plastina, R. Fazio, and G. Massimo Palma, *Phys. Rev. A* **69**, 022304 (2004).
- [56] L. Amico, F. Baroni, A. Fubini, D. Patanè, V. Tognetti, and P. Verrucchi, *Phys. Rev. A* **74**, 022322 (2006).
- [57] L. Pezzé and A. Smerzi, *Phys. Rev. Lett.* **102**, 100401 (2009).
- [58] H. Strobel, W. Muessel, D. Linnemann, T. Zibold, D. B. Hume, L. Pezzè, A. Smerzi, and M. K. Oberthaler, *Science* **345**, 424 (2014), <https://www.science.org/doi/pdf/10.1126/science.1250147>.
- [59] P. Hauke, M. Heyl, L. Tagliacozzo, and P. Zoller, *Nature Physics* **12**, 778 (2016).
- [60] P. Laurell, A. Scheie, E. Dagotto, and D. A. Tennant, *Advanced Quantum Technologies* **n/a**, 2400196, <https://onlinelibrary.wiley.com/doi/pdf/10.1002/qute.202400196>.
- [61] A. Scheie, P. Laurell, W. Simeth, E. Dagotto, and D. A. Tennant, *Materials Today Quantum* **5**, 100020 (2025).
- [62] M. Imada and M. Takahashi, *Journal of the Physical Society of Japan* **55**, 3354 (1986), <https://doi.org/10.1143/JPSJ.55.3354>.
- [63] A. Hams and H. De Raedt, *Phys. Rev. E* **62**, 4365 (2000).
- [64] S. Sugiura and A. Shimizu, *Phys. Rev. Lett.* **111**, 010401 (2013).
- [65] W. Liu, Z. Zhang, J. Ji, Y. Liu, J. Li, X. Wang, H. Lei, G. Chen, and Q. Zhang, *Chinese Physics Letters* **35**, 117501 (2018).
- [66] B. Schmidt, J. Sichelschmidt, K. M. Ranjith, T. Doert, and M. Baenitz, *Phys. Rev. B* **103**, 214445 (2021).

- [67] M. Baenitz, P. Schlender, J. Sichelschmidt, Y. A. Onyikienko, Z. Zangeneh, K. M. Ranjith, R. Sarkar, L. Hozoi, H. C. Walker, J.-C. Orain, H. Yasuoka, J. van den Brink, H. H. Klauss, D. S. Inosov, and T. Doert, *Phys. Rev. B* **98**, 220409 (2018).
- [68] R. Sarkar, P. Schlender, V. Grinenko, E. Haeussler, P. J. Baker, T. Doert, and H.-H. Klauss, *Phys. Rev. B* **100**, 241116 (2019).
- [69] L. Ding, P. Manuel, S. Bachus, F. Grubler, P. Gegenwart, J. Singleton, R. D. Johnson, H. C. Walker, D. T. Adroja, A. D. Hillier, and A. A. Tsirlin, *Phys. Rev. B* **100**, 144432 (2019).
- [70] M. M. Bordelon, E. Kenney, C. Liu, T. Hogan, L. Posthuma, M. Kavand, Y. Lyu, M. Sherwin, N. P. Butch, C. Brown, M. J. Graf, L. Balents, and S. D. Wilson, *Nature Physics* **15**, 1058 (2019).
- [71] K. M. Ranjith, D. Dmytriieva, S. Khim, J. Sichelschmidt, S. Luther, D. Ehlers, H. Yasuoka, J. Wosniza, A. A. Tsirlin, H. Kühne, and M. Baenitz, *Phys. Rev. B* **99**, 180401 (2019).
- [72] P.-L. Dai, G. Zhang, Y. Xie, C. Duan, Y. Gao, Z. Zhu, E. Feng, Z. Tao, C.-L. Huang, H. Cao, A. Podlesnyak, G. E. Granroth, M. S. Everett, J. C. Neuefeind, D. Voneshen, S. Wang, G. Tan, E. Morosan, X. Wang, H.-Q. Lin, L. Shu, G. Chen, Y. Guo, X. Lu, and P. Dai, *Phys. Rev. X* **11**, 021044 (2021).
- [73] J. Xing, L. D. Sanjeewa, A. F. May, and A. S. Sefat, *APL Materials* **9**, 111104 (2021), https://pubs.aip.org/aip/apm/article-pdf/doi/10.1063/5.0071161/14566331/111104_1_online.pdf.
- [74] T. Xie, A. A. Eberharter, J. Xing, S. Nishimoto, M. Brando, P. Khanenko, J. Sichelschmidt, A. A. Turrini, D. G. Mazzone, P. G. Naumov, L. D. Sanjeewa, N. Harrison, A. S. Sefat, B. Normand, A. M. Läuchli, A. Podlesnyak, and S. E. Nikitin, *npj Quantum Materials* **8**, 48 (2023).
- [75] Y. Li, G. Chen, W. Tong, L. Pi, J. Liu, Z. Yang, X. Wang, and Q. Zhang, *Phys. Rev. Lett.* **115**, 167203 (2015).
- [76] Y. Li, H. Liao, Z. Zhang, S. Li, F. Jin, L. Ling, L. Zhang, Y. Zou, L. Pi, Z. Yang, J. Wang, Z. Wu, and Q. Zhang, *Scientific Reports* **5**, 16419 (2015).
- [77] Y. Shen, Y.-D. Li, H. Wo, Y. Li, S. Shen, B. Pan, Q. Wang, H. C. Walker, P. Steffens, M. Boehm, Y. Hao, D. L. Quintero-Castro, L. W. Harriger, M. D. Frontzek, L. Hao, S. Meng, Q. Zhang, G. Chen, and J. Zhao, *Nature* **540**, 559 (2016).
- [78] Y. Li, D. Adroja, P. K. Biswas, P. J. Baker, Q. Zhang, J. Liu, A. A. Tsirlin, P. Gegenwart, and Q. Zhang, *Phys. Rev. Lett.* **117**, 097201 (2016).
- [79] J. A. M. Paddison, M. Daum, Z. Dun, G. Ehlers, Y. Liu, M. B. Stone, H. Zhou, and M. Mourigal, *Nature Physics* **13**, 117 (2017).
- [80] Y.-D. Li, Y.-M. Lu, and G. Chen, *Phys. Rev. B* **96**, 054445 (2017).
- [81] J. Iaconis, C. Liu, G. B. Halász, and L. Balents, *SciPost Phys.* **4**, 003 (2018).
- [82] Z. Ding, Z. Zhu, J. Zhang, C. Tan, Y. Yang, D. E. MacLaughlin, and L. Shu, *Phys. Rev. B* **102**, 014428 (2020).
- [83] M. Majumder, G. Simutis, I. E. Collings, J.-C. Orain, T. Dey, Y. Li, P. Gegenwart, and A. A. Tsirlin, *Phys. Rev. Res.* **2**, 023191 (2020).
- [84] E. Parker and L. Balents, *Phys. Rev. B* **97**, 184413 (2018).
- [85] Z. Ma, J. Wang, Z.-Y. Dong, J. Zhang, S. Li, S.-H. Zheng, Y. Yu, W. Wang, L. Che, K. Ran, S. Bao, Z. Cai, P. Čermák, A. Schneidewind, S. Yano, J. S. Gardner, X. Lu, S.-L. Yu, J.-M. Liu, S. Li, J.-X. Li, and J. Wen, *Phys. Rev. Lett.* **120**, 087201 (2018).
- [86] R. Kaneko, S. Morita, and M. Imada, *Journal of the Physical Society of Japan* **83**, 093707 (2014), <https://doi.org/10.7566/JPSJ.83.093707>.
- [87] Z. Zhu and S. R. White, *Phys. Rev. B* **92**, 041105 (2015).
- [88] W.-J. Hu, S.-S. Gong, W. Zhu, and D. N. Sheng, *Phys. Rev. B* **92**, 140403 (2015).
- [89] Y. Iqbal, W.-J. Hu, R. Thomale, D. Poilblanc, and F. Becca, *Phys. Rev. B* **93**, 144411 (2016).
- [90] S. N. Saadatmand and I. P. McCulloch, *Phys. Rev. B* **94**, 121111 (2016).
- [91] S.-S. Gong, W. Zheng, M. Lee, Y.-M. Lu, and D. N. Sheng, *Phys. Rev. B* **100**, 241111 (2019).
- [92] S. Hu, W. Zhu, S. Eggert, and Y.-C. He, *Phys. Rev. Lett.* **123**, 207203 (2019).
- [93] Y.-F. Jiang and H.-C. Jiang, *Phys. Rev. B* **107**, L140411 (2023).
- [94] B. Bernu, P. Lecheminant, C. Lhuillier, and L. Pierre, *Phys. Rev. B* **50**, 10048 (1994).
- [95] T. Jolicoeur, E. Dagotto, E. Gagliano, and S. Bacci, *Phys. Rev. B* **42**, 4800 (1990).
- [96] A. V. Chubukov and T. Jolicoeur, *Phys. Rev. B* **46**, 11137 (1992).
- [97] A. Wietek, S. Capponi, and A. M. Läuchli, *Phys. Rev. X* **14**, 021010 (2024).
- [98] For a discussion of possible valence bond state, see [97].
- [99] G. Refael and J. E. Moore, *Phys. Rev. Lett.* **93**, 260602 (2004).
- [100] Y. Imry and S.-k. Ma, *Phys. Rev. Lett.* **35**, 1399 (1975).
- [101] A. O. Scheie, Y. Kamiya, H. Zhang, S. Lee, A. J. Woods, M. O. Ajeesh, M. G. Gonzalez, B. Bernu, J. W. Villanova, J. Xing, Q. Huang, Q. Zhang, J. Ma, E. S. Choi, D. M. Pajerowski, H. Zhou, A. S. Sefat, S. Okamoto, T. Berlijn, L. Messio, R. Movshovich, C. D. Batista, and D. A. Tennant, *Phys. Rev. B* **109**, 014425 (2024).
- [102] Supplement Material (published online).
- [103] P. Hyllus, W. Laskowski, R. Krischek, C. Schwemmer, W. Wiczcerek, H. Weinfurter, L. Pezzé, and A. Smerzi, *Phys. Rev. A* **85**, 022321 (2012).
- [104] G. Tóth, *Phys. Rev. A* **85**, 022322 (2012).
- [105] S. Chakravarty, B. I. Halperin, and D. R. Nelson, *Phys. Rev. B* **39**, 2344 (1989).
- [106] A. V. Chubukov, S. Sachdev, and J. Ye, *Phys. Rev. B* **49**, 11919 (1994).
- [107] A. V. Chubukov, S. Sachdev, and T. Senthil, *Nuclear Physics B* **426**, 601 (1994).
- [108] Further analysis of the exponent α used to collapse data is provided in [102].

Can experimentally-accessible measures of entanglement distinguish quantum spin liquids from disorder-driven “random singlet” phases ?

-Supplementary information-

Tokuro Shimokawa,^{1,*} Snigdha Sabharwal,¹ and Nic Shannon¹

¹*Theory of Quantum Matter Unit, Okinawa Institute of Science and Technology Graduate University, Onna-son, Okinawa 904-0412, Japan*
(Dated: May 17, 2025)

I. EXACT DIAGONALIZATION CALCULATIONS

AT $T = 0$

The calculations of entanglement measures at $T = 0$, presented in Fig. 1 and Fig 3 of the main text, were carried out using conventional exact diagonalization (ED) methods. Within these, the Hamiltonian

$$\mathcal{H} = J_1 \sum_{\langle ij \rangle_1} (1 + \Delta \alpha_{ij}) \mathbf{S}_i \cdot \mathbf{S}_j + J_2 \sum_{\langle ij \rangle_2} (1 + \Delta \beta_{ij}) \mathbf{S}_i \cdot \mathbf{S}_j ,$$

$$\alpha_{ij}, \beta_{ij} \in [-1, 1] , \quad (\text{S1})$$

was solved on a finite cluster of size

$$N \in \{18, 24, 24, 30\} , \quad (\text{S2})$$

subject periodic boundary conditions, using a standard Lanczos algorithm, implemented through a modified version of TITPACK ver. 2 [1]. The geometries of the clusters considered is illustrated in Fig. S1.

Physical properties in the presence of disorder [$\Delta \neq 0$], were estimated by taking an average within M_N different realizations of bond-disorder $\{J_{ij}\}$, chosen from the ensemble defined in Eq. (S1). These averages were calculated as

$$\overline{\langle \hat{A} \rangle} = \frac{1}{M_N} \sum_{m=0}^{M_N-1} \langle \hat{A} \rangle^{(m)} , \quad (\text{S3})$$

where $\langle \hat{A} \rangle^{(m)}$ represents the expectation of value of an operator \hat{A} within the m^{th} realization of disorder, calculated using ED at $T = 0$, and quantum typicality methods for $T > 0$, as described below. In calculations, this average was typically calculated over

$$M_N \sim 80 \quad [N = 18] , \quad (\text{S4a})$$

$$M_N \sim 40 \quad [N = 24] , \quad (\text{S4b})$$

$$M_N \sim 20 \quad [N = 30] , \quad (\text{S4c})$$

realizations of disorder.

The model, Eq. (S1) supports four different ground states as a function of (J_1, J_2, Δ) : three-sublattice Néel order; a quantum spin liquid (QSL); stripe-like order; and a disorder-driven “random singlet” (RS) phase [cf. Fig. 2 of the main text]. The Néel, QSL and RS phases all exhibit two-point correlations which are peaked at the three-sublattice wave vector

$$\mathbf{q}_K = \left(\frac{4\pi}{3}, 0 \right) , \quad (\text{S5})$$

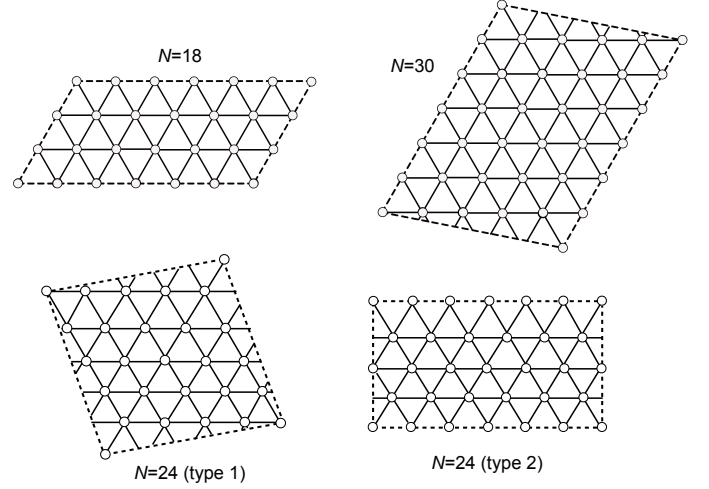


Figure S1. Finite-size clusters used in numerical calculations. Periodic boundary conditions equivalent to a torus were imposed, with the periodic boundaries illustrated through dashed lines.

(and symmetry-related wavevectors), as revealed by the equal time structure factor

$$S(\mathbf{q}) = \frac{1}{N} \langle \left| \sum_i \mathbf{S}_j e^{i\mathbf{q} \cdot \mathbf{r}_i} \right|^2 \rangle , \quad (\text{S6})$$

calculated for parameters

$$(J_1, J_2, \Delta) = (1, 0, 0) \quad [\text{Néel}] \quad (\text{S7a})$$

$$(J_1, J_2, \Delta) = (1, 0.12, 0) \quad [\text{QSL}] \quad (\text{S7b})$$

$$(J_1, J_2, \Delta) = (1, 0, 1) \quad [\text{RS}] \quad (\text{S7c})$$

and illustrated in Fig. S2.

II. DETERMINATION OF $T = 0$ PHASE TRANSITIONS THROUGH ENTANGLEMENT WITNESSES

In the main text we have argued that there are qualitative differences in concurrence (and thereby two-tangle) which distinguish quantum spin liquid (QSL) from disorder-driven “random singlet” (RS) phases [cf. Fig 1, Fig. 3 of main text]. Here we show how two different measures of entanglement, the one-tangle and two-tangle, can be used to identify the zero-temperature phase transition from Néel to RS phases as a function of disorder, in simulations of the triangular lattice model, Eq (S1).

* tokuro.shimokawa@oist.jp

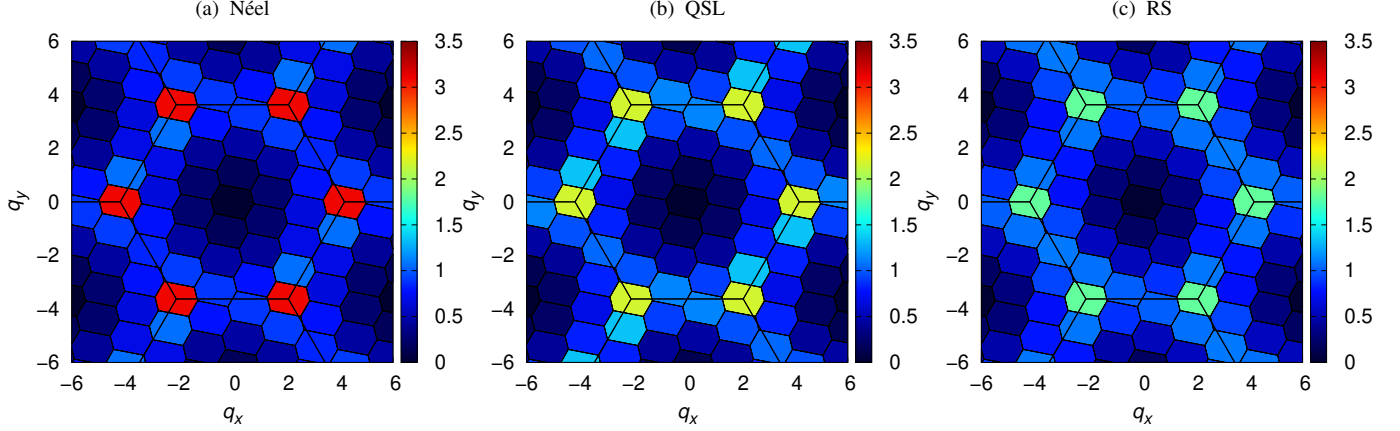


Figure S2. Comparison of correlations in Néel, quantum spin liquid (QSL) and disorder-driven “random singlet” (RS) phases, showing dominant role of fluctuations at the K-point in reciprocal space. (a) Results for equal time structure factor $S(\mathbf{q})$ [Eq. (S6)] within Néel phase, showing Bragg peaks at the three-sublattice wavevector \mathbf{q}_K [Eq. (S5)]. (b) Equivalent results for QSL, showing correlations centered on zone boundary, with maxima at \mathbf{q}_K . (c) Equivalent results for RS phase, showing diffuse correlations with maxima at \mathbf{q}_K . Results were obtained with $T = 0$ exact diagonalization (ED) calculations for the disordered triangular-lattice model, Eq. (S1), on a cluster of $N = 30$ spins [Fig. S1], with parameters Eq. (S7).

The one-tangle

$$\tau_j^{(1)} = 1 - 4\langle S_j^z \rangle^2. \quad (\text{S8})$$

provides a measure of the extent to which a single spin in a quantum spin system is entangled with other spins, under the assumption that the system has (at least) a $U(1)$ symmetry [2–4]. The entanglement measured by one-tangle may occur at any depth, i.e. involve pairs of spin, triples of spins, etc. We consider both averages of $\tau^{(1)}$ within different realizations of bond disorder

$$\overline{\tau^{(1)}} = \frac{1}{M_N} \sum_{m=0}^{M_N-1} \langle \tau_j^{(1)} \rangle^{(m)}, \quad (\text{S9})$$

and the one-tangle evaluated for correlations within a disordered state

$$\tilde{\tau}^{(1)} = 1 - 4\overline{\langle S_j^z \rangle^2}, \quad (\text{S10})$$

as measured in experiment.

Meanwhile the two-tangle

$$\tau_j^{(2)} = \sum_{i \neq j} C_{ij}^2, \quad (\text{S11})$$

is derived from concurrence,

$$C_{ij} = 2 \max\{0, \sqrt{(\langle S_i^x S_j^x \rangle + \langle S_i^y S_j^y \rangle)^2} - \sqrt{\left(\frac{1}{4} + \langle S_i^z S_j^z \rangle\right)^2 - \left(\frac{\langle S_i^z \rangle + \langle S_j^z \rangle}{2}\right)^2}\}, \quad (\text{S12})$$

and quantifies the amount of this entanglement which associated with pairs of spins, again under the assumption that the system has (at least) a $U(1)$ symmetry [2–4]. We consider

both the average of $\tau^{(2)}$ within different realizations of bond disorder

$$\overline{\tau^{(2)}} = \frac{1}{M_N} \sum_{m=0}^{M_N-1} \langle \tau_j^{(2)} \rangle^{(m)}, \quad (\text{S13})$$

and the two-tangle evaluated for correlations within a disordered state, as measured in experiment

$$\tilde{\tau}^{(2)} = \sum_{i \neq j} \tilde{C}_{ij}^2, \quad (\text{S14})$$

where

$$\tilde{C}_{ij} = 2 \max\{0, \sqrt{(\langle S_i^x S_j^x \rangle + \langle S_i^y S_j^y \rangle)^2} - \sqrt{\left(\frac{1}{4} + \langle S_i^z S_j^z \rangle\right)^2 - \left(\frac{\langle S_i^z \rangle + \langle S_j^z \rangle}{2}\right)^2}\}. \quad (\text{S15})$$

In Fig. S3 we show how disorder averages of the one-tangle and two-tangle evolve in the ground state of Eq (S1), within exact diagonalization (ED) calculations carried out for clusters of size $N = 12 \dots 30$ [Fig. S1], with parameters

$$(J_1, J_2, \Delta) = (1, 0, \Delta). \quad (\text{S16})$$

Earlier work on this model [5, 6], identified a phase transition from three-sublattice Néel to RS phases, occurring for $\Delta \lesssim 0.6$ [cf. phase diagram, Fig. 2 of main text]. This phase boundary was determined through an analysis of thermodynamic quantities [5, 6], supplemented by entanglement spectra [6].

We find that the one-tangle, $\overline{\tau^{(1)}}$ [Eq. (S9)], is weakly sensitive to the phase transition from Néel to RS ground states. In the Néel ground state, for $\Delta \lesssim 0.6$, we find $\overline{\tau^{(1)}} \equiv 1$, reflecting the fact that ground state of a finite-size cluster is a singlet,

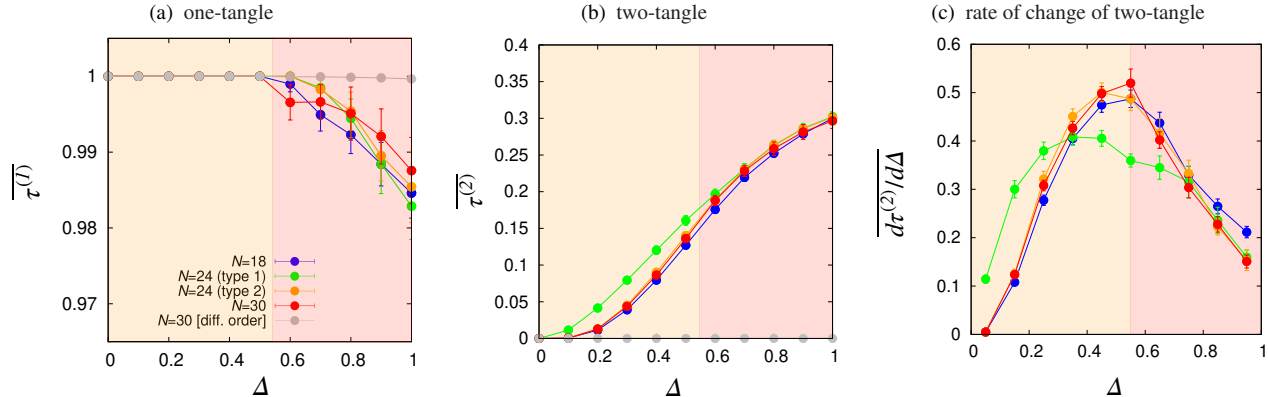


Figure S3. Determination of a zero-temperature phase transition from entanglement witnesses. (a) Dependence of the one-tangle $\overline{\tau^{(1)}}$ [Eq. (S9)] on disorder Δ , demonstrating sensitivity to the phase transition from Néel to disorder driven random singlet (RS) phases at $\Delta \approx 0.6$. When disorder averages are taken in order relevant to experiment [Eq. (S10), grey points], sensitivity to the phase transition is lost. (b) Two-tangle $\overline{\tau^{(2)}}$ [Eq. (S13)], showing evolution of two-spin entanglement as a function of disorder, Δ . The phase transition from Néel to RS ground states is distinguished by a point of inflection. When disorder averages are taken in order relevant to experiment [Eq. (S14), grey points], all sensitivity to two-spin entanglement is lost [8]. (c) First derivative of $\overline{\tau^{(2)}}$ with respect to Δ , exhibiting a maximum at the phase transition from Néel to RS ground states. Results are shown for exact diagonalization calculations of ground states of Eq. (S1), with parameters Eq. (S16).

with total spin $S = 0$, and cannot break spin-rotation symmetry. Within this Néel ground state, individual spins are both strongly, and deeply, entangled. Meanwhile in the RS ground state, for $\Delta \gtrsim 0.6$, $\overline{\tau^{(1)}}$ starts to deviate from 1, tending to a value $\overline{\tau^{(1)}} \sim 0.99$ for $\Delta \rightarrow 1$ [Fig. (S3a)]. We attribute this small reduction in the one-tangle to the existence of ground states with a finite total spin, and thereby a finite S^z , for some realizations of disorder, as previously discussed in [7]. Once the disorder averages is taken in order measured in experiment, $\overline{\tau^{(1)}}$ [Eq. (S10)], the contributions of these states sums to zero, and the one-tangle loses all sensitivity to the phase transition from Néel to RS ground states. Results for $\overline{\tau^{(1)}}$ are shown with grey circles in Fig. (S3a).

A more discriminating probe of the transition from Néel to RS phases is provided by the two-tangle $\overline{\tau^{(2)}}$ [Eq. (S13)], shown in Fig. S3b. This exhibits a point of inflection at the phase transition, $\Delta \approx 0.6$. But once again, if averages are taken in the order relevant to experiment, $\overline{\tau^{(2)}}$ [Eq. (S14), grey points], all sensitivity to two-spin entanglement is lost. The point of inflection in the two-tangle can be identified more easily if the derivative of $\overline{\tau^{(2)}}$ is taken with respect to Δ . This is illustrated in Fig. S3c.

From these results, we learn three things:

1. That measuring changes in one- and two-tangle provide a practical strategy for identifying the phase transitions into the RS phase, in simulation.
2. That measuring changes in one- and two-tangle *do not* provide a practical strategy for identifying the phase transitions into the RS phase in experiment.
3. That the RS ground state exhibits many-partite entanglement [cf. Ref. 8].

This last result follows from the fact that the two-partite

entanglement measured by the two-tangle in the RS phase $\overline{\tau^{(2)}} \sim 0.2-0.3$ does not saturate the entanglement witnessed by the one-tangle $\overline{\tau^{(1)}} \approx 1$ [2].

III. QUANTUM TYPICALITY CALCULATIONS

The direct application of exact diagonalization (ED) to quantum states at finite temperature requires a complete enumeration of states, and so is extremely memory-intensive, restricting system sizes to $N \sim 20$ spins for $S = 1/2$ systems. In this study, we have instead employed a quantum typicality method, namely, based on thermal pure quantum (TPQ) states, also known as the Hams-de Raedt method [9–15]. This approach allows the calculation of physical properties by focusing on a limited set of quantum states rather than averaging over the entire Hilbert space. As a result, it is possible to calculate thermodynamic and dynamical properties at finite temperature with high accuracy, for clusters of up to $N \sim 40$ spins. In the present study, where we address dynamical properties in the presence of disorder, calculations were carried out for clusters of $N \leq 30$ spins. These were defined on a torus with periodic boundary conditions, as illustrated in Fig. S1. In what follows, we briefly outline the essentials of the TPQ method.

The TPQ approach is based on the construction of an ensemble of thermal pure states, within which it is possible to calculate both quantum and thermal averages. We consider a system of size N , with Hilbert space dimension D , described by a Hamiltonian \mathcal{H} , at inverse temperature

$$\beta = 1/T. \quad (\text{S17})$$

States

$$|\beta, N\rangle = e^{-\beta\mathcal{H}/2}|\psi_0\rangle, \quad (\text{S18})$$

are constructed from initial vectors

$$|\psi_0\rangle = \sum_i^D c_i |i\rangle, \quad (\text{S19})$$

where the coefficients c_i are complex numbers, chosen at random, which satisfy the normalization condition

$$\sum_i |c_i|^2 = 1. \quad (\text{S20})$$

As such, $\{|i\rangle\}$ form an arbitrary orthonormal basis for the Hilbert space of the target Hamiltonian \mathcal{H} .

Within the TPQ approach, thermal expectation values of operators are estimated as averages $\langle \dots \rangle$ over I_N initial states chosen from this ensemble

$$\langle \hat{A} \rangle = \frac{\langle \beta, N | \hat{A} | \beta, N \rangle}{\langle \beta, N | \beta, N \rangle}. \quad (\text{S21})$$

The deviation of this estimator from the true expectation value can be shown to scale as

$$\Delta \langle \hat{A} \rangle \sim 1/\sqrt{I_N D} \quad (\text{S22})$$

[10]. As consequence, for a large system, accurate estimates can be obtained from a relatively small number of initial random states. In cases where the (thermal) entropy remains large at the temperatures considered, a condition commonly satisfied in frustrated systems, the number of initial vectors needed to obtain accurate estimates is particularly small [13]. In the example considered here, we find

$$I_N \lesssim \mathcal{O}(10) \quad (\text{S23})$$

is sufficient to obtain well-converged estimates.

Estimates of the dynamical structure $S(\mathbf{q}, \omega, T)$ factor can be constructed within this ensemble of thermal states, by evaluating the (real) time evolution of correlations [14]. We consider

$$\langle S_{-\mathbf{q}}^z(t=0) S_{\mathbf{q}}^z(t) \rangle = \langle \beta, N | S_{-\mathbf{q}}^z e^{i\mathcal{H}t} S_{\mathbf{q}}^z e^{-i\mathcal{H}t} | \beta, N \rangle, \quad (\text{S24})$$

where

$$S_{\mathbf{q}}^z = \frac{1}{\sqrt{N}} \sum_j S_j^z e^{i\mathbf{q} \cdot \mathbf{r}_j}, \quad (\text{S25})$$

and construct the vectors

$$|A(t)\rangle \equiv e^{-i\mathcal{H}t} | \beta, N \rangle, \quad (\text{S26})$$

and

$$|B(t)\rangle \equiv e^{-i\mathcal{H}t} S_{\mathbf{q}}^z | \beta, N \rangle. \quad (\text{S27})$$

The time-dependence of $|A(t)\rangle$ and $|B(t)\rangle$ depends on the operator $e^{-i\mathcal{H}t}$, which we resolve using a Chebyshev polynomial expansion [16]

$$e^{-i\mathcal{H}t} | \beta, N \rangle = e^{-it\bar{\lambda}} \{ J_0(\tau) + 2i^k \sum_{k=1}^m J_k(\tau) T_k(-\mathcal{H}_{\text{sc}}) \} | \beta, N \rangle, \quad (\text{S28})$$

where

$$\bar{\lambda} = \frac{1}{2}(E_{\text{max}} + E_{\text{min}}), \quad (\text{S29})$$

and

$$\delta\lambda = \frac{1}{2}(E_{\text{max}} - E_{\text{min}}), \quad (\text{S30})$$

are characteristic energy scales set by the maximal and minimal eigenvalues of the target Hamiltonian

$$\mathcal{H} | E_{\text{max}} \rangle = E_{\text{max}} | E_{\text{max}} \rangle, \text{ etc.}; \quad (\text{S31})$$

$J_k(\tau)$ is a Bessel function of the first kind;

$$\tau = \delta\lambda t, \quad (\text{S32})$$

a reduced time; and $T_k(-\mathcal{H}_{\text{sc}})$ is the k -th order Chebyshev polynomial associated with the renormalized Hamiltonian

$$\mathcal{H}_{\text{sc}} = \frac{\mathcal{H} - \bar{\lambda}}{\delta\lambda}. \quad (\text{S33})$$

The integer m in Eq. (S28) determines the order of the expansion, and is taken to be sufficiently large to ensure the convergence of results. Values of E_{max} and E_{min} can be found through a standard Lanczos calculation for the target Hamiltonian \mathcal{H} .

We determine $S^{zz}(\mathbf{q}, t, T)$ [Eq. (S24)] by constructing a discrete time series

$$\{t_i\} = \{0, \delta t, 2\delta t, \dots, t_{\text{max}}\}, \quad (\text{S34})$$

and evaluating

$$\langle B(t_i) | S_{\mathbf{q}}^z | A(t_i) \rangle \quad (\text{S35})$$

through Eq. (S26) and Eq. (S27), to obtain estimates for

$$S^{zz}(\mathbf{q}, t_i, T) \quad \forall t \in \{t_i\} \quad (\text{S36})$$

Given these results, the dynamical structure factor as function of ω can be obtained through discrete Fourier transformation

$$S^{zz}(\mathbf{q}, \omega, T) = \frac{\delta t}{\pi} \sum_{t_i > 0} \frac{\text{Re}[\langle S_{-\mathbf{q}}^z(0) S_{\mathbf{q}}^z(t_i) \rangle e^{-i\omega t_i}]}{\langle \beta, N | \beta, N \rangle} \times e^{-\frac{1}{2}(\gamma \frac{t_i}{t_{\text{max}}})^2} + \frac{\delta t}{2\pi} \frac{\langle S_{-\mathbf{q}}^z(0) S_{\mathbf{q}}^z(0) \rangle}{\langle \beta, N | \beta, N \rangle} \quad (\text{S37})$$

A Gaussian window function with

$$\gamma = 5.0 \quad (\text{S38})$$

is included to mitigate Gibbs oscillations [14]. The expectation values $\langle \dots \rangle$ are calculated using I_N initial vectors

$$I_N \sim 20 \quad [N = 18], \quad (\text{S39a})$$

$$I_N \sim 10 \quad [N = 24], \quad (\text{S39b})$$

$$I_N \sim 4 \quad [N = 30], \quad (\text{S39c})$$

following Eq. (S21), and further averaged over M different realizations of disorder, following Eq. (S13) and Eq. (S4).

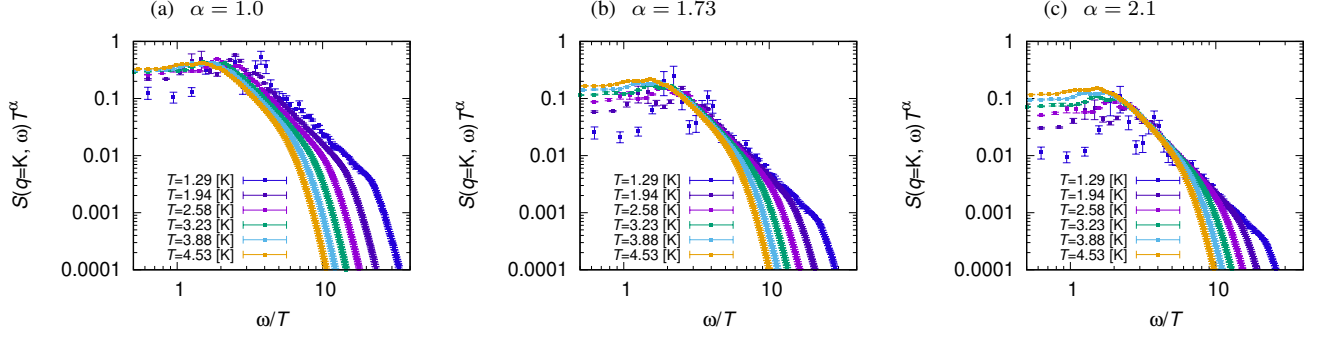


Figure S4. Scaling collapse of dynamical structure factor found in simulations of a triangular lattice antiferromagnet, as function of critical exponent, α . In all cases, data is scaled according to Eq. (S42). (a) Scaling for the value of exponent predicted by spin wave theory, $\alpha = 1.0$, showing the failure of data to collapse onto a single curve. (b) Scaling for the exponent found in experiment, $\alpha = 1.73$ [17], showing a satisfactory collapse of simulation results. (c) Scaling for exponent $\alpha = 2.1$, showing a marginally better collapse of simulation results. Results are taken from quantum typicality calculations of $S^{zz}(\mathbf{q}, \omega)$ [Eq. S37], for the minimal model of KYSe₂ [Eq. S1], with parameters taken from experiment, Eq. (S41).

We note that the duration of simulations, t_{\max} , places a bound the energy resolution which can be achieved in simulation, while the time-step, δt , determines the highest frequency which can be addressed. For the problem considered, we find

$$\delta t = 0.05 \sim 0.1 J_1^{-1}, \quad (\text{S40a})$$

$$t_{\max} = 80 \sim 100 J_1^{-1}. \quad (\text{S40b})$$

provides sufficient accuracy.

IV. DYNAMICAL SCALING OF SIMULATION RESULTS

As shown in Fig. 5 of the main text, both experimental data for KYbSe₂ [17], and simulation results for the model Eq. (S1) with parameters taken from experiment

$$(J_1, J_2, \Delta) = (1, 0.047, 0) \quad [\text{KYbSe}_2], \quad (\text{S41})$$

exhibit a scaling collapse of the dynamical structure factor $S(\mathbf{q}_K, \omega, T)$, of the form

$$T^\alpha S(\mathbf{q}_K, \omega, T) = \Phi\left(\frac{\hbar\omega}{k_B T}\right), \quad (\text{S42})$$

with exponent $\alpha = 1.73$.

In Fig. S4 we explore how this scaling collapse depends on the value of exponent α . In Fig. S4a results are shown for

the value of exponent predicted by spin wave theory, $\alpha = 1.0$ [17]. For this value of exponent, data fail to collapse onto a single curve, suggesting that spin wave theory provides a poor account of dynamics over this range of ω/T . In contrast, the value of exponent found in experiment, $\alpha = 1.73$, leads a satisfactory collapse of simulation data over the accessible range of ω/T , as shown in Fig. S4b [cf. Fig. 5(e) of the main text].

The optimal collapse of simulation data over this range of ω/T is found for $\alpha = 2.1$. This is illustrated in Fig. S4c. However the collapse of data for $\alpha = 2.1$ is only marginally better than that obtained for $\alpha = 1.73$, suggesting that results for a greater range of ω/T would be needed to make a definitive estimate of the exponent α . Since the range of ω/T available in published INS data [17] is similar to that available in simulation, this may also be true for experiment.

Notwithstanding, some difference in the value of α found in experiment and simulation might be anticipated, since the spin-rotational invariant model, Eq. (S1), is at best an approximation to anisotropic exchange interactions between Yb³⁺ ions [18]. Moreover, the fact that a scaling collapse can be obtained for a non-trivial exponent $\alpha \approx 2$ remains a striking feature of both experiment and simulation. This scaling collapse lends weight to the idea that both model [19] and material [17] lie close in parameter space to a quantum critical point.

-
- [1] H. Nishimori, [TITPACK ver. 2.](https://doi.org/10.7566/JPSJ.83.034714) (2023).
 [2] V. Coffman, J. Kundu, and W. K. Wootters, *Phys. Rev. A* **61**, 052306 (2000).
 [3] L. Amico, A. Osterloh, F. Plastina, R. Fazio, and G. Massimo Palma, *Phys. Rev. A* **69**, 022304 (2004).
 [4] L. Amico, F. Baroni, A. Fubini, D. Patanè, V. Tognetti, and P. Verrucchi, *Phys. Rev. A* **74**, 022322 (2006).
 [5] K. Watanabe, H. Kawamura, H. Nakano, and T. Sakai, *Journal of the Physical Society of Japan* **83**, 034714 (2014), <https://doi.org/10.7566/JPSJ.83.034714>.
 [6] H.-Q. Wu, S.-S. Gong, and D. N. Sheng, *Phys. Rev. B* **99**, 085141 (2019).
 [7] H. Kawamura and K. Uematsu, *Journal of Physics: Condensed Matter* **31**, 504003 (2019).
 [8] S. Sabharwal, T. Shimokawa, and N. Shannon, “Witnessing disorder in quantum magnets,” Accepted for publication in PRRsearch (2024), [arXiv:2407.20797](https://arxiv.org/abs/2407.20797) [cond-mat.str-el].
 [9] M. Imada and M. Takahashi, *Journal of the Physical Society of*

- Japan **55**, 3354 (1986), <https://doi.org/10.1143/JPSJ.55.3354>.
- [10] A. Hams and H. De Raedt, *Phys. Rev. E* **62**, 4365 (2000).
- [11] T. Iitaka and T. Ebisuzaki, *Phys. Rev. Lett.* **90**, 047203 (2003).
- [12] M. Machida, T. Iitaka, and S. Miyashita, *Phys. Rev. B* **86**, 224412 (2012).
- [13] S. Sugiura and A. Shimizu, *Phys. Rev. Lett.* **111**, 010401 (2013).
- [14] H. Ikeuchi, H. De Raedt, S. Bertaina, and S. Miyashita, *Phys. Rev. B* **92**, 214431 (2015).
- [15] H. Endo, C. Hotta, and A. Shimizu, *Phys. Rev. Lett.* **121**, 220601 (2018).
- [16] W. H. Press, S. A. Teukolsky, W. T. Vetterling, and B. P. Flannery, *Numerical Recipes: The Art of Scientific Computing (Third Edition)* (Cambridge University Press, 2007).
- [17] A. O. Scheie, E. A. Ghioldi, J. Xing, J. A. M. Paddison, N. E. Sherman, M. Dupont, L. D. Sanjeeva, S. Lee, A. J. Woods, D. Abernathy, D. M. Pajerowski, T. J. Williams, S.-S. Zhang, L. O. Manuel, A. E. Trumper, C. D. Pemmaraju, A. S. Sefat, D. S. Parker, T. P. Devereaux, R. Movshovich, J. E. Moore, C. D. Batista, and D. A. Tennant, *Nature Physics* **20**, 74 (2024).
- [18] Z. Zhu, P. A. Maksimov, S. R. White, and A. L. Chernyshev, *Phys. Rev. Lett.* **119**, 157201 (2017).
- [19] R. Kaneko, S. Morita, and M. Imada, *Journal of the Physical Society of Japan* **83**, 093707 (2014), <https://doi.org/10.7566/JPSJ.83.093707>.